# Magnetism and superconductivity in $R$PtSi ($R$=La, Ce, Nd, and Sm)

S. Ramakrishnan, K. Ghosh, Arvind D. Chinchure, V.R. Marathe, and Girish Chandra
*Tata Institute Of Fundamental Research, Bombay 400005, India*
(Received 29 March 1995; revised manuscript received 11 May 1995)

Although many studies have been made on the nonmagnetic heavy fermion CePtSi belonging to the $\alpha$-$ThSi_2$ structure, to the best of our knowledge no studies have been reported in the other rare-earth members of this series. In this paper, we report our resistivity, magnetization, and heat capacity studies on NdPtSi and SmPtSi. We have established bulk antiferromagnetic ordering in NdPtSi below 3.8 K and ferromagnetic ordering in SmPtSi below 15 K. The heat-capacity studies show large contribution from the crystal-field effects. We have also established bulk superconductivity below 3.8 K in LaPtSi from resistivity, susceptibility, and heat capacity studies. A detailed study of the influence of paramagnetic impurities (Nd and Ce) on the superconductivity of LaPtSi has been made. From this study, we are able to show that the superconducting transition temperature ($T_c$) decreases with the substitution of Nd impurities and this can be explained using Abrikosov and Gor'kov theory. On the other hand, Ce impurities show large depression of $T_c$ which we ascribe to the Kondo effect due to Ce atoms with the Kondo temperature, $T_k \approx 0.25T_c$. The observed data have been analyzed using recent quantum Monte Carlo calculations by Jarrel for superconductors with arbitary $T_k$ values.

## I. INTRODUCTION

A large number of equiatomic ternary silicides and germanides has been made[1] and many Ce-containing samples of these series have been studied extensively.[2] They display many interesting properties such as mixed valence, Kondo lattice formation, and antiferromagnetic and ferromagnetic ordering at low temperatures. However, only a few studies have been made to understand the magnetic ordering exhibited by the other rare-earth members (such as Pr, Nd, and Sm) of this series. It has been known for some time that $R$PtSi ($R$=La, Ce, Pr, Nd, Sm, and Gd) compounds form in a derivative of the $\alpha$-$ThSi_2$ structure.[3] Tetragonal $\alpha$-$ThSi_2$ (space group $I4_1md$) is an interesting structure because of the possibility that one can replace 50% of the Si atoms by other elements in an ordered fashion. In the case of the $R$PtSi ($R$=La,Ce, Pr, Nd, Sm, and Gd) series, Pt and Si atoms are arranged in an ordered fashion on the Si sites such that each Pt atom has three close neighbors of Si and vice versa. Of this series, CePtSi is now established as a heavy fermion system with a nonmagnetic ground state.[4–9] This compound is estimated to have a Kondo temperature of 6.7 K.[10] It is found that the replacement of Si by Pt in $CeSi_{2-x}Pt_x$ changes both the Kondo temperature and the $\gamma$ value from 200 K and 104 $mJ/molK^2$ (for $x$=0) to 5 K and 700 $mJ/molK^2$ (for $x = 1.0$), respectively.[11] Although the configurations of the Ce ions are same in both compounds ($x$=0 and $x$=1), the large change in the physical properties emphasizes the importance of ligand ions surrounding Ce ions. The literature survey indicates that a number of studies[4–9] have been made on CePtSi. However, to the best of our knowledge no detailed studies have been reported for other rare-earth members of this series. In this paper we report on resistivity [$\rho$(T)] and susceptibility [$\chi(T)$] studies from 2 to 300 K on NdPtSi and SmPtSi. We also present the dc magnetization and heat-capacity studies on these compounds from 2 to 40 K. Similar studies on PrPtSi will be reported elsewhere. Earlier studies[3–5] have indicated that LaPtSi belonging to the $\alpha$-$ThSi_2$ structure is a superconductor with a $T_c$ of 3.3 K. A recent resistivity study has quoted[6] a higher value of 3.7 K for the $T_c$ of a sample of LaPtSi. In this paper, we establish the bulk superconductivity in LaPtSi by performing resistivity, susceptibility, and heat-capacity studies. Since the Kondo temperature of CePtSi is of the same order as the superconducting transition temperature ($T_c$) of LaPtSi, one should observe a rapid decrease of $T_c$ with the substitution of Ce for La in LaPtSi. To understand the influence of the effect of Ce and Nd substitution for La on the normal state and the superconducting state properties in LaPtSi, a detailed study has been undertaken and the results are analyzed in terms of the existing theories.

## II. EXPERIMENTAL DETAILS

Samples belonging to the series $R$PtSi ($R$=La, Ce, Nd, and Sm) and $La_{1-x}R_xPtSi$ ($R$= Ce and Nd) were made by melting the individual constituents (taken in stoichiometric proportions) in an arc furnace under a high-purity argon atmosphere. The purity of La, Ce, Nd, Sm, and Pt was 99.9% whereas the purity of Si was 99.999%. The alloy buttons were remelted 5–6 times to ensure proper mixing. The samples were annealed at 700 °C for SmPtSi and 850 °C for other samples for 2 weeks. The x-ray powder diffraction pattern of the samples did not show the presence of any parasitic impurity phases and the lattice constants $a$ and $c$ obtained by us are given in Table I. Their values are in agreement with the previ-

 

TABLE I. Structural properties of $R$PtSi ($R$=La, Ce, Nd, and Sm).

| Sample | $a$ (Å) | $c$ (Å) |
|---|---|---|
| LaPtSi | 4.2494(4) | 14.5388(4) |
| CePtSi | 4.1979(4) | 14.4884(4) |
| NdPtSi | 4.1628(4) | 14.4152(4) |
| SmPtSi | 4.1232(4) | 14.3742(4) |

ously published values.[3] The temperature dependence of susceptibility ($\chi$) was measured using a superconducting quantum interference device magnetometer (Quantum Design, model MPMS) in a field of 5 kOe in the temperature range from 2 to 300 K. The ac susceptibility was measured using a home-built susceptometer[12] from 1.5 K to 5 K. The resistivity was measured using a four-probe dc technique with contacts made using an ultrasonic soldering iron (with nonsuperconducting solder) on a cylindrical sample of 2 mm diameter and 10 mm length. The temperature was measured using a calibrated Si diode (Lake Shore Inc.) sensor. The sample voltage was measured with a nanovoltmeter (Keithley model 182) with a current of 25 mA using a 20 ppm stable (Hewlett Packard model) current source. All the data were collected using an IBM compatible PC/AT via an IEEE-488 interface. The heat capacity in zero field between 2 and 40 K was measured using an automated adiabatic heat pulse method. A calibrated germanium resistance thermometer (Lake Shore Inc.) was used as the temperature sensor in this range.

## III. RESULTS AND DISCUSSION

### A. Magnetization studies

#### 1. *Magnetization studies on NdPtSi*

The temperature dependence of the inverse susceptibility ($1/\chi$) of the NdPtSi sample from 2 to 300 K is shown in Fig. 1. The inset shows the $1/\chi$ behavior of the same sample at low temperature on an expanded scale. The data clearly show an anomaly around 3.8 K which we have identified as the antiferromagnetic ordering temperature ($T_n$). The $\chi$ data from 100 to 300 K fit well to the Curie-Weiss relation

$$\chi = \frac{C}{(T-\theta_p)}, \qquad (1)$$

where $C$ is given by $C = \mu_{\text{eff}}^2/8$. The best fit (which is shown as a solid line in Fig. 1) is found for a $\theta_p$ value of $-2.89$ K and an effective $Nd^{3+}$ ion moment of $3.68\mu_B$. The addition of a temperature-independent $\chi_0$ term did not improve the quality of the fit and gave an extremely small value for the $\chi_0$ term. Therefore, the fit was made only to the Curie-Weiss relation. The computed effective moment is equal to the free ion moment of $Nd^{3+}$, which is $3.62\mu_B$. Below 100 K, the temperature dependence

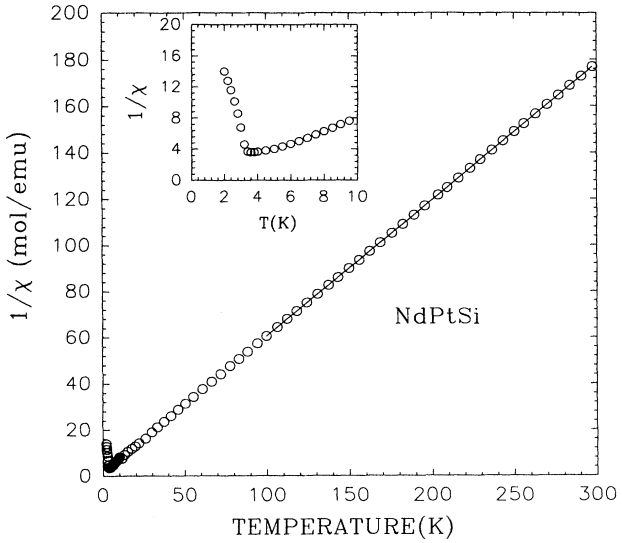


FIG. 1. Variation of inverse susceptibility ($1/\chi$) of NdPtSi from 2 to 300 K. The insets show the low-temperature $1/\chi$ data. The solid line indicates the fit to Curie-Weiss law from 100 to 300 K.

of $1/\chi$ deviates from linearity, which could be due to crystal-field effects.

The isothermal magnetization ($M$ vs $H$) data on NdPtSi from 0 to 5 T at 2.0 K (below $T_n$) and 10 K (well above $T_n$) are shown in Fig. 2. The $M$ vs $H$ data at 2.0 K show possible metamagnetic transitions at 1 and 2.5 T. The nature of the antiferromagnetism at low fields and the observed metamagnetic transitions at high fields

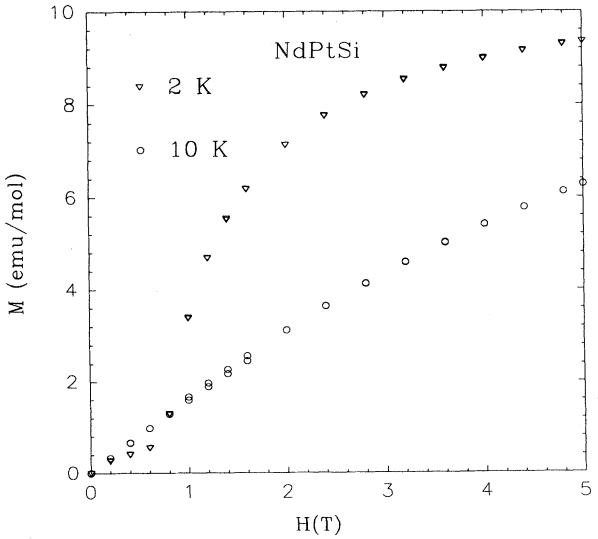


FIG. 2. Isothermal magnetization ($M$ vs $H$) plot of NdPtSi at 2 K and 10 K. No hysteresis is observed in the forward and reverse legs of magnetization.

can be understood only by the neutron diffraction studies on this sample. Another interesting aspect of the magnetization studies is the observation of nonlinearity in the $M$ vs $H$ plot at 10 K. In general, one expects a linear plot when the sample is in the paramagnetic state. The observed nonlinearity in the magnetization (although not very large) could be either due to the presence of strong antiferromagnetic correlations or due to crystal-field effects. Even here, neutron measurements will be helpful to resolve this issue.

#### 2. *Magnetization studies on SmPtSi*

The temperature dependence of the inverse susceptibility ($1/\chi$) of the SmPtSi sample from 2 to 300 K is shown in Fig. 3. The two insets show the $1/\chi$ behavior of the same sample at low temperatures on an expanded scale. The data clearly show an anomaly around 15 K and a rapid increase in susceptibility below 40 K. At high temperatures, the curve does not follow the Curie-Weiss expression which is typical of samarium compounds. The isothermal magnetization data at 5, 10, and 25 K are shown in Fig. 4. The magnetization at 5 K tends to saturate in a 5 T field and the observed hysteresis in the forward and reverse legs seems to suggest ferromagnetic ordering in this sample. The same situation is present at 10 K although the hysteresis is slightly reduced. Well above the transition temperature (observed from $\chi$ data), the magnetization is clearly linear and reversible, which suggests that the sample is already in the paramagnetic state at 25 K. The observed linearity in $M$ vs $H$ at 25 K contrasts the nonlinearity observed in NdPtSi.

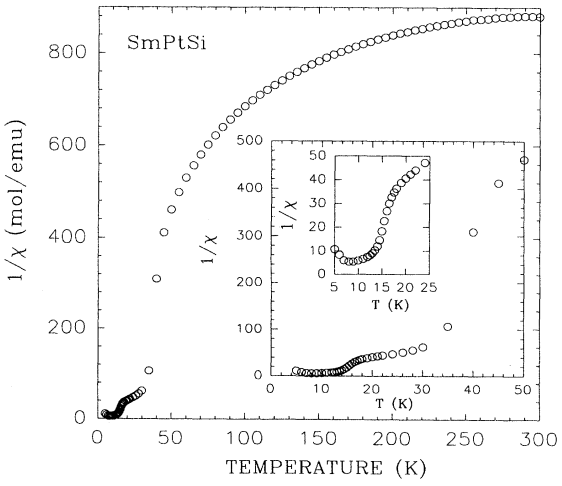


FIG. 3. Variation of inverse susceptibility ($1/\chi$) of SmPtSi from 2 to 300 K. The insets show the low temperature $1/\chi$ data.

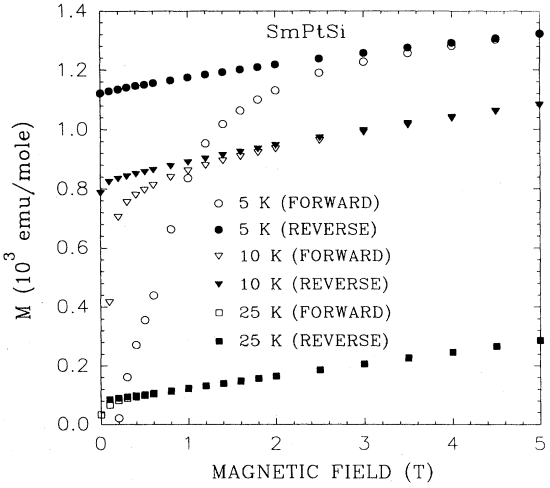


FIG. 4. Isothermal magnetization ($M$ vs $H$) plot of SmPtSi at 2, 10, and 25 K. Hyteresis in the forward and reverse legs of magnetization is observed at 5 K and 10 K and no hysteresis is observed at 25 K.

### B. Resistivity studies

#### 1. *Resistivity studies on NdPtSi*

The temperature dependence of the resistivity ($\rho$) of NdPtSi is shown in Fig. 5. The inset shows the low-temperature $\rho$ data on an expanded scale. One can see the change in slope of the $\rho$ vs $T$ curve at 3.8 K. The $\chi$ data also show an anomaly at this temperature. The $\rho$ decreases rapidly below this temperature. This dependence could be fitted to a power-law relation from 1.5 K

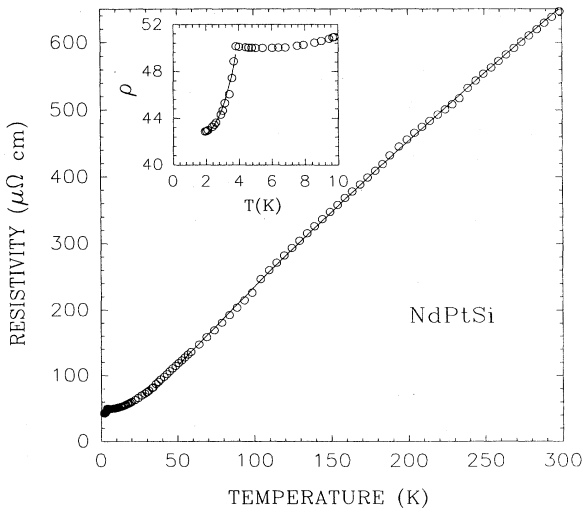


FIG. 5. Temperature dependence of resistivity ($\rho$) of NdPtSi from 2 to 300 K. The inset shows the low-temperature $\rho$ data from 2 to 10 K. The solid lines are fit to the models (see text).

to 3.8 K, which can be written as

$$\rho = \rho_0 + a\,T^n \,. \tag{2}$$

The values of $\rho_0$ and $a$ are found to be 42.6 $\mu\Omega$ cm and 8.6 n$\Omega$ cm/K$^5$, respectively. The optimum value of $n$ was close to 5. In antiferromagnets, one observes a $T^3$ dependence of $\rho$ below $T_n$. At present, we have not understood the reason for this abrupt fall and the $T^5$ power-law dependence of the resistivity below $T_n$. Resistivity studies on single crystals of this sample are required to understand this $\rho$ behavior.

At high temperatures (50 K< $T$ <300 K), the $\rho$ data significantly deviate from the linear temperature dependence. Such a deviation from linear temperature dependence at high temperatures has been seen in many alloys where the saturation is attributed to the high value of $\rho$ of these alloys at these temperatures. This behavior is also seen in previous studies on silicides and germanides.[13,14] One of the models which describes the $\rho(T)$ of these compounds is known as the parallel resistor model.[15] In this model the expression of $\rho(T)$ is given by

$$\frac{1}{\rho(T)} = \frac{1}{\rho_1(T)} + \frac{1}{\rho_{\max}} \,, \tag{3}$$

where $\rho_{\max}$ is the saturation resistivity which is independent of temperature and $\rho_1(T)$ is the ideal temperature-dependent resistivity. Further, the ideal resistivity is given by the following expression:

$$\rho_1(T) = \rho_0 + C_1 \left(\frac{T}{\theta_D}\right)^3 \times \int_0^{\theta_D/T} \frac{x^3 dx}{[1-\exp(-x)][\exp(x)-1]} \,, \tag{4}$$

where $\rho(0)$ is the residual resistivity and the second term is due to phonon-assisted electron scattering similar to the $s$-$d$ scattering in transition metal alloys. $\theta_D$ is the Debye temperature and $C_1$ is a numerical constant. The resistivity data fitted to the above equations in the range 50 – 300 K yielded $\rho_0$ =62 $\mu\Omega$ cm and $\Theta_D$ = 220 K, which is close to the measured value of 225 K by a heat-capacity study (see below).

#### 2. *Resistivity studies on SmPtSi*

The temperature dependence of the resistivity ($\rho$) of SmPtSi is shown in Fig. 6. The inset shows the low-temperature $\rho$ data on an expanded scale. One can see the change in slope of the $\rho$ vs $T$ curve at 15 K. The $\chi$ data also show an anomaly at this temperature. The $\rho$ decreases below this temperature. This dependence of $\rho$ between 2 and 12 K is fitted to Eq. (2) and the best fit was made with $n$ = 4, $\rho_0$=36.6 $\mu\Omega$ cm, and $a$=0.6 n$\Omega$ cm/K$^4$. In the case of ferromagnetic ordering one observes a $T^2$ dependence of resistivity which arises mainly due to electron-magnon scattering.[16] Hence the observed $T^4$ dependence is a quite unusual phenomenon. However, such a dependence could arise due to large anistropy in the resistivity. Resistivity measurements on single crystals are required to settle this issue.

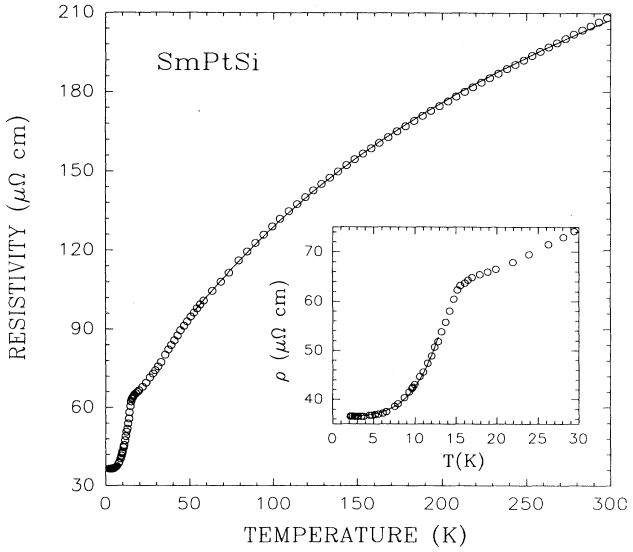


FIG. 6. Temperature dependence of resistivity ($\rho$) of SmPtSi from 2 to 300 K. The inset shows the low-temperature $\rho$ data from 2 to 20 K. The solid lines are fit to the models (see text).

At high temperatures, the $\rho$ data show a deviation from the linear temperature dependence similar to that of NdPtSi. We have fitted the data to the parallel resistor model and the best fit is obtained for $\rho_0$ =90 $\mu\Omega$ cm and $\Theta_D$ = 230 K, which is close to the measured value of 235 K by a heat-capacity study (see below).

### C. Heat-capacity studies

#### 1. *Heat-capacity studies on NdPtSi*

The temperature dependence of $C_p$ from 2 to 35 K of NdPtSi is shown in Fig. 7. The inset shows the low-temperature $C_p$ data. The large jump at 3.6 K ($\Delta C$= 6.3 J/mol K) clearly shows bulk magnetic ordering in this sample. This temperature is slightly lower than the $T_n$ value observed from the $\chi$ as well $\rho$ measurements. From these observations, we conclude that this sample undergoes antiferromagnetic ordering below 3.8 K. The magnetic contribution to the heat capacity (which is obtained after subtracting the measured $C_p$ data from that of LaPtSi) is shown in Fig. 8. The calculated entropy is also shown in the same figure. The increase in the entropy at high temperatures ($T$ >20 K) signifies contribution from crystal-field effects in this sample. The total entropy below $T_n$ is found to be 4 J/mol K, which is close to $R$ ln2, and this shows that the ground state is a doublet. Preliminary calculations suggest that the next excited state is also a doublet and its separation from this doublet ground state is approximately 60 K. An exact calculation of the crystal-field contribution to the heat-

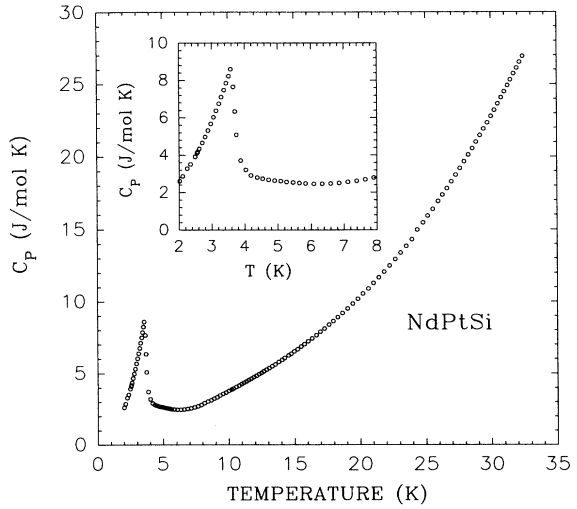


FIG. 7. Plot of $C_p$ vs $T$ of NdPtSi from 2 to 35 K. The inset shows the same plot from 2 to 8 K.

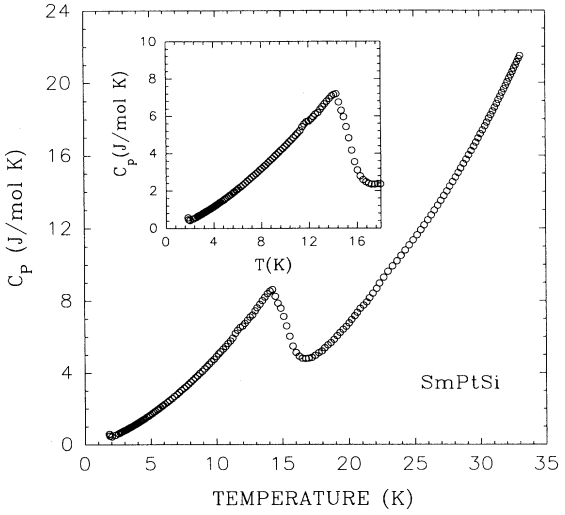


FIG. 9. Plot of $C_p$ vs $T$ of SmPtSi from 2 to 35 K. The inset shows the same plot from 2 to 20 K.

capacity, susceptibility, and resistivity requires a detailed model which is in progress and will be published elsewhere. From the high-temperature heat-capacity data, we estimate the Debye temperature for this sample to 225 K, which agrees with the result obtained from the resistivity analysis.

### 2. *Heat-capacity studies on SmPtSi*

The temperature dependence of $C_p$ from 2 to 35 K of SmPtSi is shown in Fig. 9. The inset shows the low-temperature $C_p$ data. The large jump at 14.4 K ($\Delta C$= 4.2 J/mol K) clearly shows bulk magnetic ordering in this sample. Since one observes a saturation in the magnetization at low temperatures (5 and 10 K) with hysteresis, we conclude that Sm spins are undergoing a ferromagnetic transition below 14.4 K. The magnetic contribution to the heat capacity (which is obtained after subtracting the measured $C_p$ data from that of LaPtSi) is shown in Fig. 10. The calculated entropy is also shown in the same figure. The increase in the entropy at high temperatures ($T$ >20 K) signifies a contribution from crystal-field effects in this sample. The total entropy below $T_c$ is found to be 5 J/mol K, which is slightly higher than $R\ln 2$, and this shows that the ground state is a doublet. An exact calculation of the crystal-field contribution to the heat-capacity, susceptibility, and resistivity requires a detailed

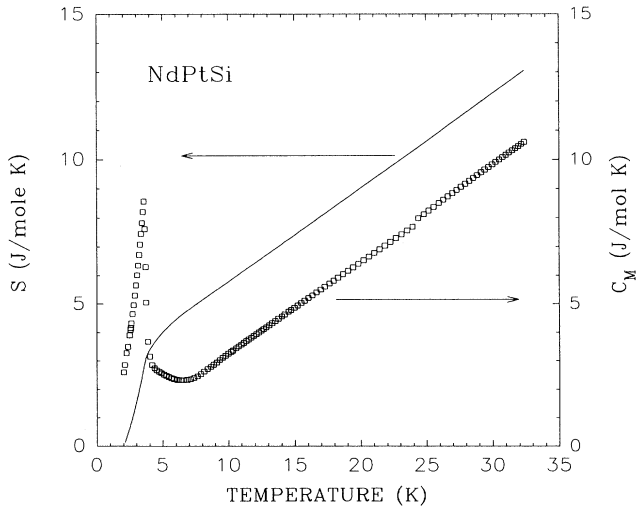


FIG. 8. Plot of magnetic contribution to the heat capacity ($C_m$) vs $T$ of NdPtSi from 2 to 35 K. The solid line is the magnetic contribution to the entropy ($S$).

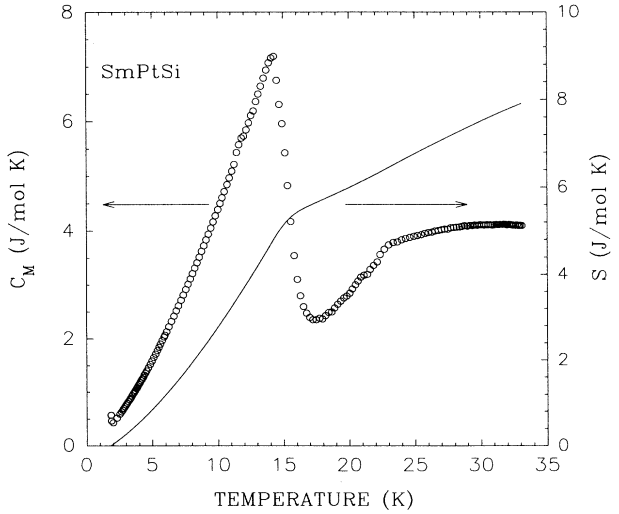


FIG. 10. Plot of magnetic contribution to the heat capacity ($C_m$) vs $T$ of SmPtSi from 2 to 35 K. The solid line is the magnetic contribution to the entropy ($S$).

model which is in progress and will be published elsewhere. From the high-temperature heat-capacity data, we estimate the Debye temperature for this sample to 235 K, which agrees with the result obtained from the resistivity analysis.

### D. Normal and superconducting state properties of LaPtSi

#### 1. Magnetic susceptibility studies

The temperature dependence of the dc magnetic susceptibility ($\chi_{dc}$) of the LaPtSi sample in a field of 5 kOe from 2 to 300 K is shown in Fig. 11. The inset shows the ac susceptibility behavior of the same sample at low temperature in an ac field of 2 Oe. This inset clearly shows the diamagnetic transition below 3.8 K which is slightly higher than the previously reported value.[6] The normal state $\chi_{dc}$ of this sample has a temperature-independent value of $5.8\times10^{-5}$ emu/mol down to 50 K. Below 50 K, there is an increase in $\chi_{dc}$ which we attribute to the presence of paramagnetic impurities in this sample. The temperature-independent $\chi_{dc}$ has contributions from the core diamagnetism, Landau diamagnetism, and Pauli paramagnetism. They can be expressed as

$$\chi_{dc} - \chi_{core} = S\,(\chi_{Landau} + \chi_{Pauli})\,, \qquad (5)$$

where $S$ is the Stoner enhancement factor. This can be further simplified as

$$\chi_{dc} - \chi_{core} = S\,\chi_{Pauli}\left[1 - \frac{1}{3}\left(\frac{m}{m_b}\right)\right]\,, \qquad (6)$$

where $\chi_{Pauli} = n\,N_A\mu_B^2 N(E_F)$ is the Pauli susceptibility, $\mu_B$ is the Bohr magneton, $m$ is the free electron mass, and $m_b$ is the band mass. Assuming the valence of La as 3, Pt as 2, and Si as 4, we estimate the core diamagnetism to be $-2.8\times10^{-5}$ emu/mol. We have also calculated the value of the Pauli susceptibility as $2.7\times10^{-5}$ emu/mol and this yields a value of 3.2 for the Stoner factor of LaPtSi.

#### 2. Resistivity studies

The temperature dependence of the resistivity ($\rho$) of LaPtSi is shown in Fig. 12. The insets show the low-temperature $\rho$ data on an expanded scale. The $\rho$ data show a jump at 3.8 K which is the superconducting transition temperature ($T_c$) of this sample. This is in agreement with the $T_c$ value obtained from $\chi$ data. In the normal state (4.5 K$< T <$25 K), the temperature dependence of the $\rho$ could be fitted to Eq. (2) which yields an optimum value for $n$ of 3 and the values of $\rho_0$ and $a$ are found to be 18.8 $\mu\Omega$ cm and 0.6 $n\Omega\,\mathrm{cm/K^3}$, respectively. This value of $n$ agrees with the Wilson's $s$-$d$ scattering model which predicts a $T^3$ dependence of $\rho(T)$ for $T < \theta_D/10$.

At high temperatures (50 K$< T <$300 K), the $\rho$ data significantly deviate from the linear temperature dependence similar to that of other $R$PtSi compounds. The resistivity data fitted to the above equations in the range 50 – 300 K yielded $\rho_0$ =19 $\mu\Omega$ cm and $\Theta_D$ = 250 K which is close to the measured value of 244 K by a heat-capacity study which will be described in the following section.

#### 3. Heat-capacity studies

The temperature dependence of the heat capacity ($C_p$) from 2 to 35 K of LaPtSi is shown in Fig. 13. The

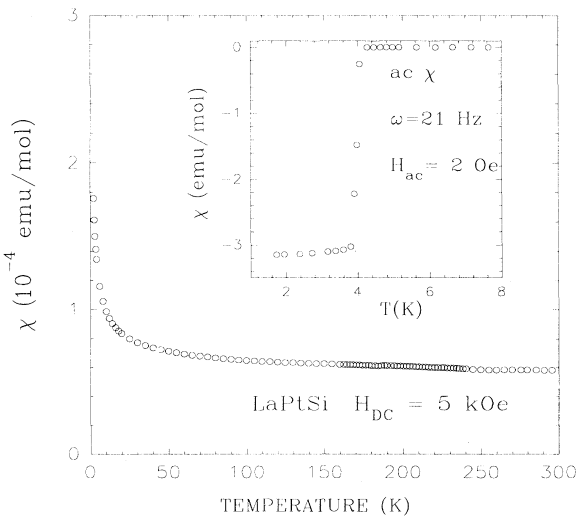


FIG. 11. Variation of dc susceptibility ($\chi$) of LaPtSi from 2 to 300 K in a field of 5 kOe. The inset shows the low-temperature ac susceptibility data.

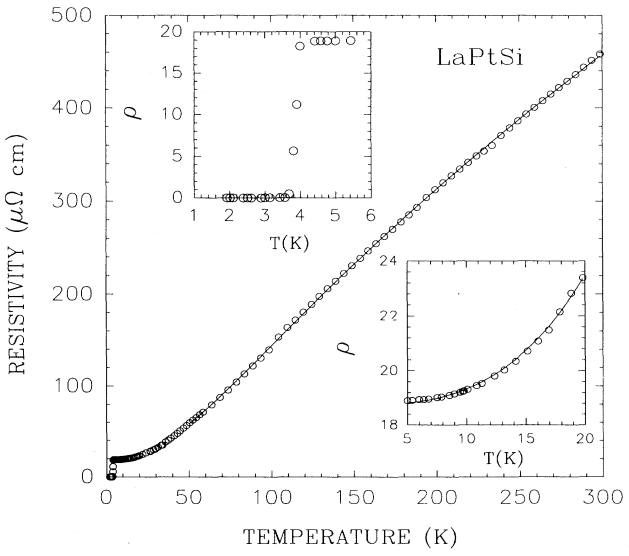


FIG. 12. Temperature dependence of resistivity ($\rho$) of LaPtSi from 2 to 300 K. The insets show the low-temperature $\rho$ data from 2 K to 5 K and 6 K to 25 K. The solid lines are fit to the models (see text).

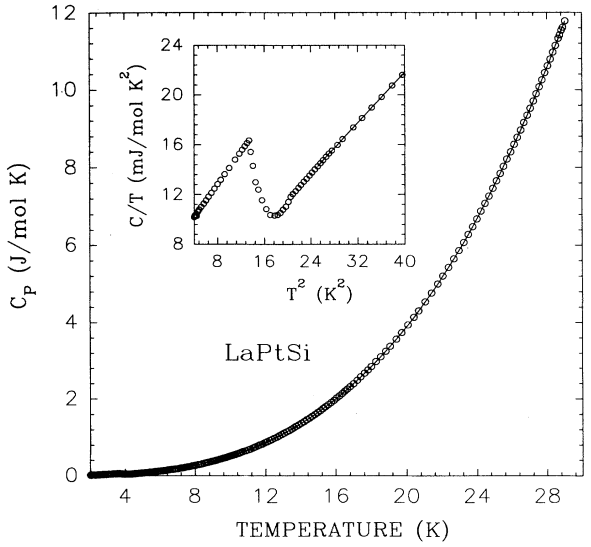


FIG. 13. Plot of $C_p$ vs $T$ of LaPtSi from 2 to 35 K. The inset shows the same plot from 2 K to 8 K.

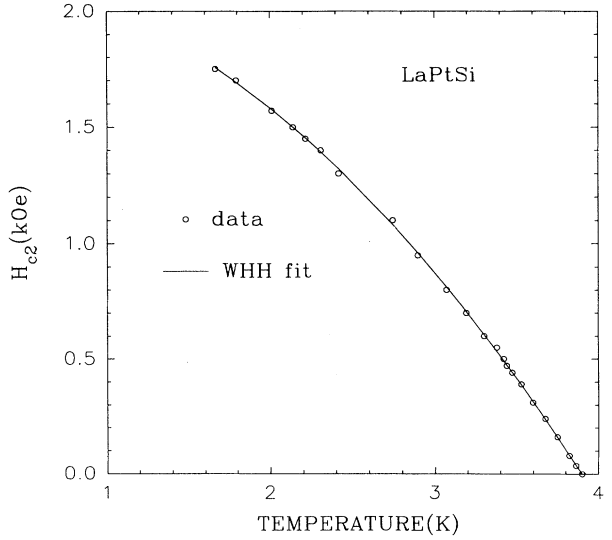


FIG. 14. Temperature dependence of the upper critical field ($H_{c_2}$) of LaPtSi from 3.8 to 1.4 K. Solid line is a fit to the WHH model.

inset shows the low-temperature $C_p/T$ vs $T$ data. The jump in $C_p$ at 3.8 K ($\Delta C$= 18 mJ/mol K) clearly shows bulk superconducting ordering in this sample below this temperature. The temperature dependence of $C_p$ is fitted to the expression,

$$C_p = \gamma T + \beta T^3 , \tag{7}$$

where $\gamma$ is due to electronic contribution and $\beta$ is due to the lattice contribution. The value of the ratio $\Delta C_p/\gamma T_c$ is 1.3, which shows that the sample is a weak coupling BCS superconductor. The fit to the heat capacity data [using Eq. (7)] in the temperature range from 5 to 20 K yielded 3.56 mJ/mol K$^2$ and 0.477 mJ/mol K$^4$ for $\gamma$ and $\beta$, respectively. The $\gamma$ value has been obtained by matching the entropy of normal and superconducting states at $T_c$ as suggested by Stewart *et al.*[17] From the $\beta$ value of 0.40 mJ/mol K$^4$, we estimate the $\theta_D$ to be 244 K using the relation,

$$\theta_D = \left(\frac{12\,\pi^4\,N\,r\,k_B}{5\beta}\right)^{1/3} , \tag{8}$$

where $N$ is the Avogadro's number, $r$ is the number of atoms per formula unit, and $k_B$ is Boltzmann's constant.

#### *4. Upper critical field studies*

The estimation of the upper critical field ($H_{c_2}$) values at a given temperature has been made by measuring the resistance of the sample under a given magnetic field. The transition temperature in a given field is defined as the temperature which corresponds to the midpoint of the resistance jump. The temperature dependence of $H_{c_2}$ is shown in Fig. 14. We have fitted this temperature dependence of $H_{c_2}$ to Werthamer-Helfand-Hohenberg theory (WHH),[18] which incorporates the spin-orbit scattering term ($\lambda_{s.o.}$) in a dirty type. We obtain a value of 2 for $\lambda_{s.o.}$, 2.18 kOe for $H_{c_2}(0)$ and 0.8 T/K for $dH_{c_2}/dT$ near $T_c$. The value of the Pauli paramagnetic limiting field ($H_{\text{Pauli}}$=1.84$T_c$) for LaPtSi is very large (7.2 T) compared to the estimated value of the upper critical field at 0 K. This could be the reason for the absence of Pauli paramagnetic limiting in the upper critical field of this compound. One can also estimate the $dH_{c_2}/dT$ using the relation,

$$dH_{c_2}/dT = 4.48\,\gamma\,\rho\,(\text{T/K}) , \tag{9}$$

where $\gamma$ is the electronic heat-capacity coefficient (ergs/cm$^3$ K$^2$) and $\rho$ ($\Omega$ cm) is the residual resistivity. Substituting the values of $\gamma$ and $\rho$, we get a value 0.75 T/K which is close to the value obtained from WHH theory.

### E. Estimation of normal and superconducting states parameters

Using the value of $\theta_D$ and $T_c$, we can estimate the electron-phonon scattering parameter $\lambda$ from McMillan's theory[19] where $\lambda$ is given by the relation

$$\lambda = \frac{1.04 + \mu^* \ln(\theta_D/1.45\,T_c)}{(1 - 0.62\,\mu^*)\ln(\theta_D/1.45\,T_c) - 1.04} . \tag{10}$$

Assuming $\mu^*$=0.1, we find the value of $\lambda$ to be 0.56 which puts LaPtSi as an intermediate coupling superconductor. On the basis of purely thermodynamical arguments, the thermodynamic critical field at $T$=0 K [$H_c(0)$] can be determined by integrating the entropy difference between

the superconducting and normal states. From our experimental heat capacity data, we obtain a value of 480 Oe for $H_c(0)$. One can also calculate the thermodynamical critical field $H_c(0)$ from the expression[20]

$$H_c(0) = 4.23\ \gamma^{1/2}\ T_c\ , \tag{11}$$

where $\gamma$ is the heat capacity coefficient(erg/cm$^3$ K$^2$). This gives a value of $H_c(0)$ of 483 Oe. We can estimate the Ginzburg-Landau coherence length $\xi_{GL}$ at $T$=0 K from the relation

$$\xi_{GL}(0) = \frac{8.57 \times 10^{-7}}{[\gamma\ \rho\ T_c]^{1/2}}\ , \tag{12}$$

where $\gamma$ and $\rho$ are the electronic heat capacity coefficient (erg/cm$^3$ K$^2$) and resistivity ($\Omega$ cm) of the sample just above $T_c$. This equation yields a value of 338 Å for $\xi_{GL}(0)$.

Using the expression $\kappa = 7.49 \times 10^3\ \gamma^{1/2}\ \rho$ (where $\kappa = \lambda_{GL}/\xi_{GL}$), we get a $\kappa$ value of 4.2. From the value of $\xi_{GL}(0)$ = 338 Å (determined earlier), we get a value of 1425 Å for the Ginzburg-Landau penetration depth $\lambda_{GL}(0)$. The lower critical value can be determined by using the relation

$$H_{c_1}(0) = \frac{H_c\ (0)\ \ln(\kappa)}{2^{1/2}\ \kappa}\ , \tag{13}$$

which yields a value of 117 Oe for the lower critical field at 0 K. This value of $H_{c_1}(0)$ has to be verified with magnetization measurements on the same sample. Such measurements on this sample are in progress and they will be reported elsewhere. The enhanced density of states can be calculated using the relation

$$N^*(E_F) = 0.2121\ \gamma/N\ , \tag{14}$$

where $N$ is the number of atoms per formula unit and $\gamma$ is expressed in mJ/mol K$^2$. The value of $N^*(E_F)$ is 0.24 states/[eV atom (spin-direction)] and the value of the bare density of states $N(E_F) = N^*(E_F)/(1+\lambda)$ = 0.15 states/[eV atom (spin direction)].

The parameters are calculated using the Ginzburg-Landau theory for dirty superconductors. To verify the self-consistency of our approach, we have estimated the mean free path ($l$) of our sample using the expression

$$l = 1.27 \times 10^4\ [\rho\ n^{2/3}\ (S/S_F)]^{-1}\ , \tag{15}$$

where $n$ is the conduction electron density in units of cm$^{-3}$ and $S/S_F$ is the ratio of the area of the Fermi surface to that of a free electron gas of density $n$. If one assumes a simple model of a spherical Fermi surface ($S/S_F$=1), the value of $l$ would be 43 Å and one can also calculate the value of the BCS coherence length (for $S/S_F$=1) from the expression,

$$\xi_0 = 7.95 \times 10^{-17}\ [n^{2/3}]\ (\gamma\ T_c)^{-1}\ , \tag{16}$$

where $\gamma$ is expressed in ergs/cm$^3$ K$^2$. The value of $\xi_0$ was found to be 3642 Å which is much higher than $l$ which implies LaPtSi is a dirty type-II superconductor. Using this $l$ value, $\xi_0$ can be compared with that obtained from the expression

$$H_{c_2}(0) = \frac{\phi_0}{4.54\ \xi_0\ l}\ , \tag{17}$$

which yields a value of 4800 Å for $\xi_0$. The normal and superconducting state parameters are listed in Table II.

TABLE II. Superconducting and normal state properties of LaPtSi.

| Parameter | Units | Value |
|---|---|---|
| $T_C$ | K | 3.9 |
| $\gamma$ | mJ/mol K$^2$ | 3.56 |
| $\beta$ | mJ/mol K$^4$ | 0.477 |
| $\theta_D$ | K | 250 |
| $\lambda$ | | 0.56 |
| $N^*(E_F)$ | states/(eV atom spin) | 0.24 |
| $N(E_F)$ | states/(eV atom spin) | 0.15 |
| $\xi_{GL}(0)$ | Å | 338 |
| $\lambda_{GL}(0)$ | Å | 1425 |
| $H_{c_2}(0)$ | Oe | 2180 |
| $H_{c1}(0)$ | Oe | 117 |
| $H_c(0)$ | Oe | 480 |
| $l$ | Å | 43 |
| $\xi_0^{BCS}$ | Å | 3642 |
| $\xi_0$ | Å | 4800[a] |
| $S$ | | 3.2 |

[a]Estimated from Eq. (16).

### F. Normal state properties of $La_{1-x}R_xPtSi$ ($R$=Ce and Nd)

#### 1. *Magnetic susceptibility studies*

The temperature dependence of the inverse susceptibility ($1/\chi$) for $La_{1-x}Ce_xPtSi$ and $La_{1-x}Nd_xPtSi$ is shown in Fig. 15 and Fig. 16, respectively. The temperature dependence of $\chi$ data from 100 to 300 K can be fitted to the Curie-Weiss relation given by Eq. (1). The values of $\theta_p$, $\mu_{eff}$, and $x$ for both Ce and Nd series are given in Table III. The effective magnetic moments are found to be around 3.62$\mu_B$ for Nd and 2.56$\mu_B$ for Ce ions. The addi-

TABLE III. Magnetic properties of $La_{1-x}M_xPtSi$ ($M$=Ce and Nd).

| Sample | $\mu_{eff}$ | $\theta_p$ |
|---|---|---|
| CePtSi | 2.56$\mu_B$ | −39 K |
| $La_{0.9}Ce_{0.1}PtSi$ | 2.55$\mu_B$ | −35 K |
| $La_{0.97}Ce_{0.03}PtSi$ | 2.54$\mu_B$ | −32 K |
| NdPtSi | 3.62$\mu_B$ | −2.9 K |
| $La_{0.2}Nd_{0.8}PtSi$ | 3.64$\mu_B$ | −2.2 K |
| $La_{0.7}Nd_{0.3}PtSi$ | 3.63$\mu_B$ | −2 K |
| $La_{0.9}Nd_{0.1}PtSi$ | 3.64$\mu_B$ | −1 K |

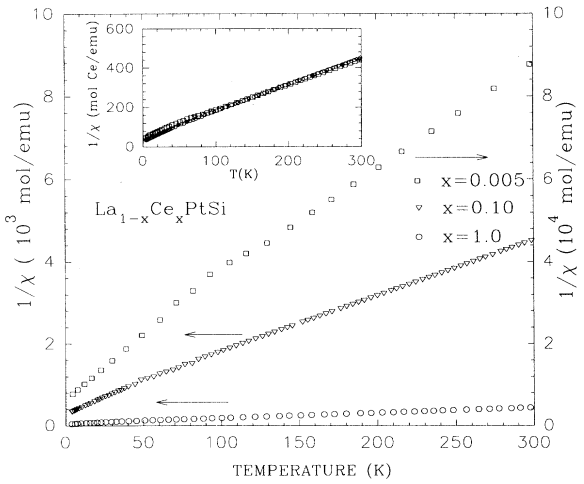


FIG. 15. Variation of inverse susceptibility $(1/\chi)$ of $La_{1-x}Ce_xPtSi$ from 2 to 300 K. The inset shows the $\chi$ values of $x$=0.1 and $x$=0.005, scaled to 1 mol of Ce.

tion of a temperature-independent $\chi_0$ term to Eq. (1) did not improve the quality of the fit and gave an extremely small value for the $\chi_0$ term. Therefore, the fit was made only to the Curie-Weiss relation. The computed effective moments observed are very close to their respective free ion moments ($Nd^{3+}$ and $Ce^{3+}$). Below 100 K, the temperature dependence of $1/\chi$ deviates from linearity which could be due to crystal-field effects. In the case of the $La_{1-x}Ce_xPtSi$ system, both $\mu_{eff}$ and $\theta_p$ do not change significantly with the increase of the Ce concentration. From this one can conclude that the RKKY interaction (in this system) is weak and the dilute Kondo state is continuously connected to the dense Kondo state as a linear function of Ce atoms. Similar conclusions have been drawn in other Kondo lattice systems.[21–23]

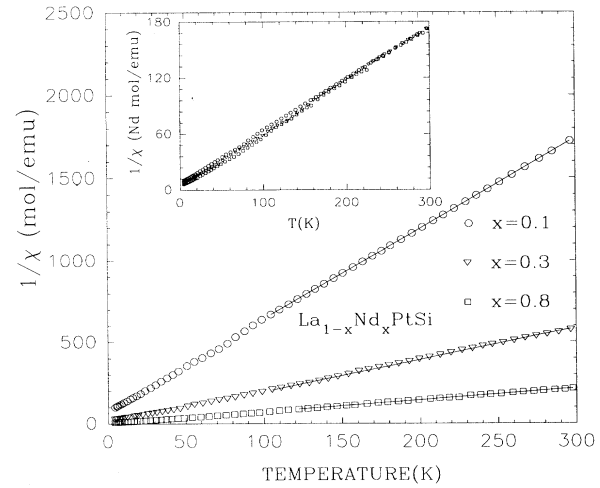


FIG. 16. Variation of inverse susceptibility $(1/\chi)$ of $La_{1-x}Nd_xPtSi$ from 2 to 300 K. The inset shows the $\chi$ data scaled to 1 mol Nd.

### 2. *Resistivity studies*

The temperature dependence of the resistivity ($\rho$) for $La_{1-x}Ce_xPtSi$ and $La_{1-x}Nd_xPtSi$ is shown in Fig. 17 and Fig. 18, respectively. The magnetic contribution to the resistivity of CePtSi increases up to 30 K of CePtSi and rapidly falls below 19 K which is in agreement with previous studies. On the other hand, the sample $La_{0.9}Ce_{0.1}PtSi$ shows a resistivity (Kondo) minimum around 19 K which reduces to 2.5 K in the dilute limit of $x$=0.003 (not shown here). The low-temperature data are fitted to Hamann's model[24,25] expression (for $x$=0.1 in LaPtSi) and from this fit we deduce a value of 6 K for $T_k$ which is closer to the value reported in a previous study.[11] The magnetic part of the resistivity is shown as an inset in Fig. 17. The theoretical fit is shown as a solid line in the same inset. The resistivity data of $La_{1-x}Nd_xPtSi$ show normal behavior at low temperature and deviation from linear temperature dependence at high temperatures as we have seen in the LaPtSi sample. The low-temperature data show a power law dependence [see Eq. (2)] with $n$ =3.2 for $x$=0.1. The high-temperature data could be fitted to the parallel resistor model with $\rho_0$ =67.5 $\mu\Omega$ cm and $\theta_D$ = 246 K. The solid lines correspond to the fit to the parallel resistor model from 50 to 300 K.

### 3. *Heat-capacity studies*

The temperature dependence of the magnetic heat capacity ($C_m$) (after the subtraction of $C_p$ of LaPtSi) from 2 to 30 K of CePtSi and $La_{0.9}Ce_{0.1}PtSi$ is shown in Fig. 19. The inset shows the low-temperature $C_p/T$ vs $T$ data for both samples. The heat-capacity data of CePtSi

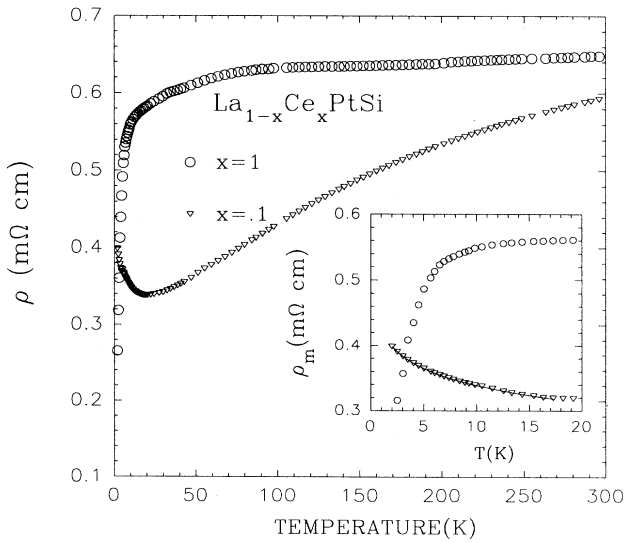


FIG. 17. Temperature dependence of resistivity ($\rho$) of $La_{1-x}Ce_xPtSi$ from 2 to 300 K. The inset shows the low-temperature $\rho$ data from 2 to 10 K. The solid line is a fit to Hamann's model (see text).

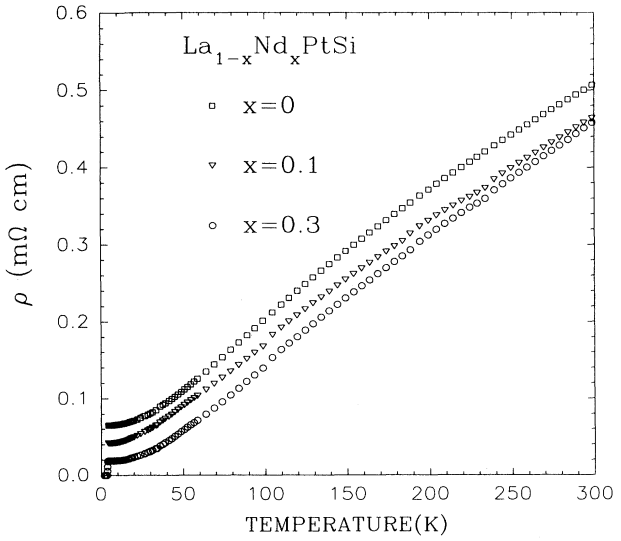


FIG. 18. Temperature dependence of resistivity ($\rho$) of $La_{1-x}Nd_xPtSi$ from 2 to 300 K. The inset shows the low-temperature $\rho$ data from 2 to 20 K. The solid lines are a fit to a model (see text).

are in agreement with earlier studies.[5,6] The heat capacity of $La_{0.9}Ce_{0.1}PtSi$ has been scaled to 1 mol of Ce. The scaling of heat capacity data for $x$=0.1 and $x$=1 for the $La_{1-x}Ce_xPtSi$ system suggests that the heavy fermion behavior observed in CePtSi can be explained using single-ion behavior. This behavior is quite similar to other studies in the Ce system.[21–23]

### G. Superconductivity in $La_{1-x}R_xPtSi$ ($R$=Ce and Nd)

The $T_c$ dependence on the impurity concentration in $La_{1-x}Nd_xPtSi$ and $La_{1-x}Ce_xPtSi$ is shown in Fig. 20 and Fig. 21, respectively. In the case of $La_{1-x}Nd_xPtSi$, the $T_c$ depression is expressed in terms of the magnetic pair breaking theory of Abrikosov and Gor'kov (AG),[27] which is given by the equation[28]

$$\ln(T/T_c) = \psi(0.5) - \psi(0.5+\Gamma) , \quad (18)$$

where $\psi$ is the digamma function and $\Gamma$ is the pair breaking parameter which is given by

$$\Gamma = 0.14\ (\alpha/\alpha_{cr})\ (T_{c0}/T_c) = 0.14\ (n/n_{cr})\ (T_{c0}/T_c) , \quad (19)$$

where $n_{cr}$ is given by

$$n_{cr} = k_B T_{c0}/4\gamma_E\ N(0)\ J_{sf}^2\ (g_J-1)^2\ J(J+1) , \quad (20)$$

where $\gamma_E$ is the Euler's constant, $N(0)$ is the density of states of the parent compound, and $J_{sf}$ is the interaction parameter between conduction electrons and the rare earth spin. In the limit $n \to 0$, the rate of decrease of $T_c$ with Nd concentration $x$ can be written as,

$$\frac{dT_c}{dn} = 3\,\frac{dT_c}{dx} = -(\pi^2/2)\ N(0)\ k_B^{-1}\ J_{sf}^2\ (g_J-1)^2\ J(J+1) . \quad (21)$$

Assuming the values of $J$ = 9/2, $g_J$=8/11, N(0)=0.24, and $dT_c/dx$ = 0.21 K/at. % of Nd, we estimate the value of $J_{sf}$ as 50 meV. The solid line in the Fig. 20 is a fit to AG theory and the critical concentration is found to be 12.8 at. %. The $T_c$ vs $x$ data could also be fitted by taking the crystal-field effects into consideration us-

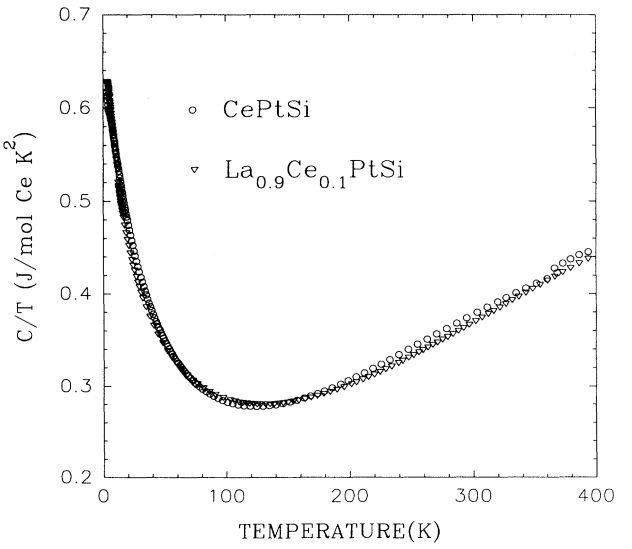


FIG. 19. Plot of magnetic contribution to the heat capacity ($C_m$) vs $T$ of $La_{1-x}Ce_xPtSi$ from 2 to 20 K. The $C_m$ for $x$=0.1 is scaled to one mol of Ce.

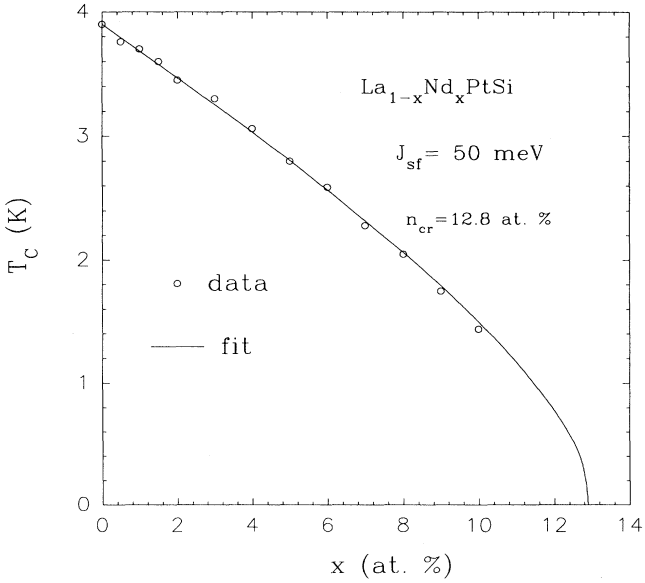


FIG. 20. Variation of the superconducting transition temperature ($T_c$) with the Nd concentration $x$ in $La_{1-x}Nd_xPtSi$. The solid line is a fit to the model (see text).

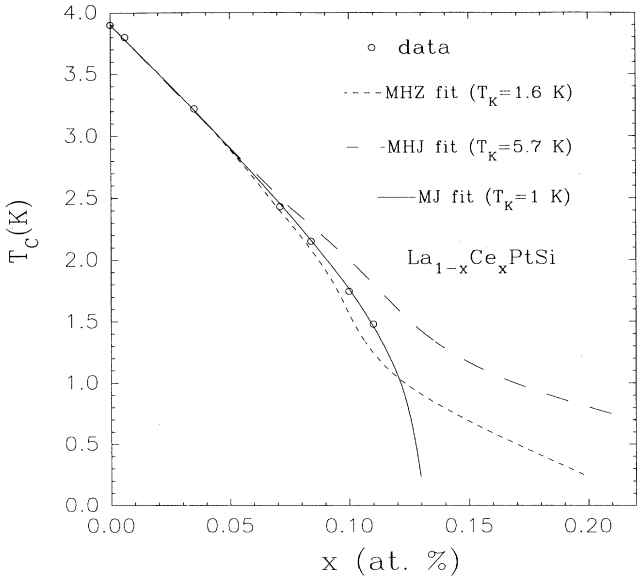


FIG. 21. Variation of the superconducting transition temperature ($T_c$) with Ce concentration $x$ in $La_{1-x}Ce_xPtSi$. The solid line is a fit to the Jarrel (MJ) model and the dashed and dotted lines are fits to the MHZ model (see text).

ing the formalism proposed by Fulde and Peschel.[29] The crystal-field parameters were obtained from the analysis of the Schottky anomaly observed in the heat-capacity data and the high-temperature magnetic susceptibility data.[30] We get a value of 75 meV for $J_{sf}$ from this fit. However, the quality of this fit is poor compared to that of simple AG theory. The value of $J_{sf}$, although large, is comparable to those obtained by others in rare-earth intermetallic borides and stannides.[31,32] The large value of $J_{sf}$ results in the fall of $T_c$ with $x$ which explains why we could not observe coexistence of superconductivity and antiferromagnetism in $La_{1-x}Nd_xPtSi$ above 0.6 K.

The rapid fall of $T_c$ with Ce impurities is evident from Fig. 21 and this is due to the fact that the $T_k$ of the $La_{1-x}Ce_xPtSi$ system is close to the $T_c$ of pure LaPtSi. Although the estimated $T_k$ for the $x$=0.1 sample is close to that of CePtSi, in the dilute limit ($x$ <0.01), the $T_k$ is estimated to be around 1 K from the resistivity analysis. A similar variation in $T_k$ has also been reported in other Kondo lattice systems.[21,26] Since $T_k/T_{c0}<1$, the temperature dependence of $T_c$ with the Ce concentration is fitted to MHZ theory,[33] which is again given by Eq. (18) with $\Gamma$ defined as

$$\Gamma = \frac{T_c}{T_{c0}} \frac{c}{(2\pi)^2 N_0 T_{c0}} (1 - y_0^2) , \qquad (22)$$

where c is the impurity concentration. $y_0^2$ is defined as

$$y_0^2 = \frac{\pi^2 S(S+1)}{\ln^2 T_c/T_K + \pi^2 S(S+1)}. \qquad (23)$$

The solid line in the Fig. 21 is a fit to Eq. (18) with $\Gamma$ given by Eq. (22). The critical concentration is found to be 0.3 at. % of Ce (extrapolated value) with an initial decrease of 14 K/at. % which is lower than experimentally observed value of 16.7 K. The value of $T_k$ from this fit (shown as a dotted line in Fig. 11) is found to be 1.6 K which is higher than the value of 1 K obtained from resistivity studies on dilute samples ($x$ <0.01). However, for slightly higher values of Ce impurities MHZ theory deviates significantly from the observed values with a change over to positive curvature for $T_c/T_{c0}<0.2$. We have also made an attempt to fit our data with $T_k$ as 6 K using MHZ theory. This fit is shown as dashed lines in Fig. 21. However, our measurements on a sample with 0.2 at. % of Ce did not show superconductivity down to 0.6 K. It is now well known that MHZ theory fails to account for the $T_c$ depression when $T_c/T_k \approx 1$,[34] and even when $T_c/T_k<1$, the value of $T_c/T_{c0}$ is strongly dependent on $\lambda$, the electron-phonon coupling constant.[35,36] A recent quantum Monte Carlo analysis[35–37] predicts a different functional dependence of $T_c/T_{c0}$ with $x$. According to Jarrel,[37] the initial dependence can be written as

$$N(0)\, k_B\, (dT_c/dc) = g(T_K/T_{c0})\, f(\lambda_0) , \qquad (24)$$

where $g(T_k/T_{c0})$ and $f(\lambda_0)$ are universal functions whose forms are given by him.[37] Using the values of N(0), $T_{c0}$, and $T_k$, we estimate the value of the initial slope as −16.8 K which is in agreement with the observed value (16.7 K). The solid line in the Fig. 21 is a fit from Jarrel's theory appropriately scaled to match $T_k$ and $\lambda$ of our data. The fact that our data fit well to his theory reaffirms that the ratio $T_c/T_{c0}$ depends also on the value of $\lambda$ [namely, the weak coupling superconductors ($\lambda$ <1) show a strong depression with Kondo impurities compared to the strong coupling ones ($\lambda$>1)]. According to Jarrel,[37] the maximum depression occurs when $T_c$=$T_k$ which is different from the value estimated in previous models.[33,34] Recent numerical renormalization group studies are in agreement with Jarrel's calculations.[38,39]

## IV. CONCLUSION

To conclude, we have measured the magnetic susceptibility, resistivity, and heat-capacity of NdPtSi and SmPtSi. The NdPtSi sample undergoes antiferromagnetic ordering below 3.8 K. The resistivity decreases rapidly below $T_n$ which is not understood. In the case of $NdSi_2$ (Refs. 40, 41) (which forms in a distorted $\alpha$-$ThSi_2$ structure), Nd moments order antiferromagnetically around 10 K. Moreover, the resistivity below $T_n$ behaves as $T^3$ which is attributed to electron-magnon scattering. So the removal of Si as one goes from $NdSi_2$ to NdPtSi results in a reduction of the ordering temperature of Nd spins. This is in contrast with the observation in $CeSi_2$ and CePtSi where the magnetism becomes stronger with Pt substitution for Si. In the case of SmPtSi, we observe ferromagnetic ordering below 14.4 K whereas in $SmSi_2$, there is no magnetic ordering down to 4.2 K (Sm is thought to be divalent in this case).[41] The heat-capacity data of both samples show a signifi-

cant contribution from crystal-field effects which requires further studies. The $\rho$'s of the two samples show an anomalous power law dependence below their respective ordering temperatures which is not understood at this moment. Further, NdPtSi shows a nonlinear $M$ vs $H$ response in the paramagnetic region ($T$=10 K) which requires further study. We have also shown the existence of bulk superconductivity in LaPtSi below 3.9 K from resistivity, susceptibility, and heat-capacity studies. A detailed study of the influence of Ce and Nd impurities on the $T_c$ of LaPtSi has been made. For Ce, we observe a sharp fall of $T_c$ which we attribute to the Kondo effect. Our data of $T_c/T_{c0}$ with $x$ fit fairly well to Jarrel's theory compared to the usual MHZ theory. We have estimated the Kondo temperature to be 1 K from Jarrel's theory[37] and resistivity studies. We also observe an AG-type pair breaking effect with Nd impurities and the estimated value of the $J_{sf}$ is 50 meV. With the inclusion of crystal-field effects, the value of $J_{sf}$ is increased to 75 meV. According to a recent theory by Kim and Overhauser,[42] even the AG formalism underestimates the $T_c$ depression by a factor $1/\lambda$, in which case, the value of $J_{sf}$ would be 37.4 meV for the simple AG theory (without crystal-field effects) and 56.3 meV with a crystal-field contribution. Electron-paramagnetic-resonance (EPR) measurements with Gd (since GdPtSi also forms in the same structure) will help here to get an independent estimate of $J_{sf}$ to resolve this issue.


[1] E. Hovestreydt, N. Engel, K. Klepp, B. Chabot, and E. Parthe, J. Less-Common Met. **86**, 247 (1982).
[2] T. Fujita, T. Suzuki, S. Nishigori, T. Takabatake, H. Fujii, and J. Sakurai, J. Magn. Magn. Mater. **108**, 35 (1992).
[3] K. Klepp and E. Parthe, Acta Crystallogr. **38**, 1105 (1982).
[4] J. Evers, G. Oehlinger, A. Weis, and C. Probst, Solid State Commun. **50**, 61 (1984).
[5] H.F. Braun, J. Less-Common Met. **100**, 105 (1984).
[6] W.H. Lee and R.N. Shelton, Phys. Rev. B **35**, 5369 (1987).
[7] M. Sera, T. Satoh, and T. Kasuya, Jpn. J. App. Phys. Suppl. **26**, 551 (1987).
[8] M. Sera, T. Satoh, and T. Kasuya, J. Phys. Soc. Jpn. **56**, 1932 (1987).
[9] R. Köhler, B. Strobel, C. Kämmerer, A. Grauel, U. Gottwick, E. Göring, A. Höhr, G. Sparn, C. Geibel, and S. Horn, J. Magn. Magn. Mater. **90 & 91**, 428 (1990).
[10] L. Rebelsky, K. Reilly, S. Horn, H. Borges, J.D. Thompson, J.O. Willis, R. Aikin, R. Caspari, and C.D. Bredl, J. Appl. Phys. **63**, 3405 (1988).
[11] N. Sato, M. Kohgi, T. Satoh, Y. Ishikawa, H. Hiroyoshi, and H. Takei, J. Magn. Magn. Mater. **52**, 360 (1985).
[12] S. Ramakrishnan, S. Sundaram, R.S. Pandit, and Girish Chandra, J. Phys. E **18**, 650 (1985).
[13] S. Ramakrishnan, K. Ghosh, and Girish Chandra, Phys. Rev. B **45**, 10769 (1992).
[14] K. Ghosh, S. Ramakrishnan, and Girish Chandra, Phys. Rev. B **48**, 10440 (1993).
[15] H. Wiesmann, M. Gurvitch, H. Lutz, A.K. Ghosh, B. Schwarz, M. Strongin, P.B. Allen, and J.W. Halley, Phys. Rev. Lett. **38**, 782 (1977).
[16] N. Rivier and A.E. Mensah, Physica B **91**, 85 (1977).
[17] G.R. Stewart, G.P. Meisner, and H.C. Ku, in *Proceedings of the IVth International Conference on d- and f-band Superconductivity*, edited by W. Buckel and W. Weber (Kernforschungszentrum, Karlsruhe, 1982), p. 81.
[18] N.R. Werthamer, E. Helfand, and P.C. Hohenberg, Phys. Rev. **147**, 295 (1966).
[19] W.L. McMillan, Phys. Rev. **167**, 331 (1967).
[20] T.P. Orlando, E.J. McNiff, Jr., S. Foner, and M.R. Beasley, Phys. Rev. B **19**, 4545 (1979).
[21] N. Sato, S. Kunii, I. Oguro, T. Komatsubara, and T. Kasuya, J. Phys. Soc. Jpn. **53**, 3967 (1984).
[22] Y. Onuki, Y. Shimizu, M. Nishihara, Y. Machii, and T. Komatsubara, J. Phys. Soc. Jpn. **54**, 1964 (1985).
[23] C.L. Lin, A. Wallash, J.E. Crow, T. Mihalisin, and P. Schlottmann, Phys. Rev. Lett. **58**, 1232 (1987).
[24] D.R. Hamann, Phys. Rev. **158**, 570 (1967).
[25] P.E. Bloomfield and D.R. Hamann, Phys. Rev. B **164**, 856 (1967).
[26] F.G. Aliev, N.B. Brandt, V.V. Molschalkov, and S.M. Chundinov, J. Low Temp. Phys. **57**, 61 (1984).
[27] A.A. Abrikosov and L.P. Gor'kov, Sov. Phys. JETP **12**, 1243 (1961).
[28] For an excellent review on the effect of magnetic impurities on superconductivity of metallic alloys, see M.B. Maple, J. App. Phys. **9**, 179 (1976).
[29] P. Fulde and I. Peschel, Adv. Phys. **21**, 1 (1972).
[30] A. Chinchure, K. Ghosh, S. Ramakrishnan, V.R. Marathe, and Girish Chandra (unpublished).
[31] H.B. MacKay, L.D. Woolf, M.B. Maple, and D.C. Johnston, J. Low Temp. Phys. **41**, 639 (1980).
[32] S.K. Malik, A.M. Umarji, and G.K. Shenoy, Phys. Rev. B **32**, 4426 (1985).
[33] E. Müller-Hartmann, in *Magnetism*, edited by H. Suhl (Academic Press, New York, 1973), Vol. V, p. 353.
[34] T. Matsuura, S. Ichinose, and Y. Nagaoka, Prog. Theor. Phys. **57**, 713 (1977).
[35] M. Jarrel, Phys. Rev. Lett. **61**, 2612 (1988).
[36] M. Jarrel, in *Computer Simulation Studies in Condensed Matter Physics*, edited by D.P. Landau, K.K. Mon, and H.B. Schüttler (Springer-Verlag, Berlin, 1990), Vol. II, p. 137
[37] M. Jarrel, Phys. Rev. B **41**, R4815 (1990).
[38] K. Satori, H. Shiba, O. Sakai, and Y. Shimizu, J. Phys. Soc. Jpn. **9**, 3239 (1992).
[39] H. Shiba, K. Satori, O. Sakai, and Y. Shimizu, Physica B **186-188**, 239 (1993).
[40] I.P. Mayer, E. Banks, and B. Post, J. Phys. Chem. **66**, 693 (1962).
[41] S. Labroo, X. Zhang, P. Hill, and N. Ali, J. Less-Common Met. **149**, 337 (1989).
[42] Yong-Jihn Kim and A.W. Overhauser, Phys. Rev. B **49**, 15799 (1994).